ISSN 1063-7834, Physics of the Solid State, 2010, Vol. 52, No. 9, pp. 1787–1796. © Pleiades Publishing, Ltd., 2010.
Original Russian Text © D.L. Khalyapin, P.D. Kim, J. Kim, I.A. Turpanov, A.Ya. Beten'kova, G.V. Bondarenko, T.N. Isaeva, I. Kim, 2010, published in Fizika Tverdogo Tela, 2010, Vol. 52, No. 9, pp. 1665–1674.

METALS
AND SUPERCONDUCTORS

Effect of Alloy Formation Processes in the Co–Cu System on the Magnetic and Magnetoresistance Properties of Multilayer Co/Cu Films with Ultrathin Co Layers Prepared by DC Magnetron Sputtering

D. L. Khalyapin[a, b, *], P. D. Kim[b], J. Kim[c], I. A. Turpanov[b], A. Ya. Beten'kova[b], G. V. Bondarenko[b], T. N. Isaeva[b], and I. Kim[d]

[a] *Siberian Federal University, pr. Svobodny 79, Krasnoyarsk, 660041 Russia*

* *e-mail: dimlh@iph.krasn.ru*

[b] *Kirensky Institute of Physics, Siberian Branch, Russian Academy of Sciences, Akademgorodok 50, Krasnoyarsk, 660036 Russia*

[c] *Department of Metallurgical and Material Science, Hanyang University, Sa-3-dong 1271, Ansan, 426-791 Korea*

[d] *EMD Laboratory, Central R&D Institute, Samsung Electro-Mechanics Co., LTD, 314 Maetan3-Dong, Yeongtong-Gu, Suwon, Gyunggi-Do, 443-743 Korea*

Received November 23, 2009

Abstract—This paper reports on a study of multilayer Co/Cu films with an effective thickness of the Co layer of ~3.5 Å, which were prepared by magnetron sputtering. The samples prepared have been found to have a metastable multiphase structure. An analysis of the data obtained by structural and, primarily, by magnetic methods has revealed that the main phases are the Co/Cu supersaturated solid solution (alloy) with a Co concentration of about 30 at %, the superparamagnetic phase, and the paramagnetic phase, which is accounted for by the presence of small (a few atoms at most) Co clusters embedded in the Cu matrix. A clearly pronounced maximum in the temperature dependences of the low-field magnetoresistance has been found, which is associated with the temperature of the magnetic phase transition of the supersaturated Co–Cu alloy.

DOI: 10.1134/S1063783410090015

1. INTRODUCTION

Multilayer Co/Cu films and granular alloys of this system have been enjoying widespread research interest from the time these materials had revealed the giant magnetoresistance effect (GMR) [1–3]. It was originally believed that GMR structures based on the Co/Cu system should possess sharp interfaces, as well as a high stability, because of the extremely low mutual solubility of cobalt and copper, which is well seen from the equilibrium phase diagram [4]. Recent intensive experimental studies have revealed, however, a rich variety of structural imperfections, such as mixing at the interface, mutual diffusion, etc., which can primarily be traced to the technique employed in their preparation and which affect markedly the physical properties of the material, in particular, the magnitude of the GMR effect [5]. Even in MBE-grown multilayers, interface mixing does occur because of the surface energies of cobalt and copper being different [6–8]. To better understand the magnetic and magnetic-transport properties of such structures, one has to invoke quite frequently models based on mechanisms atypical of an ideal multilayer structure, such as the effect of a superparamagnetic phase [9], existence of a direct exchange coupling through pinholes [10], and magnetic dipole interaction between asperities of two adjacent interfaces [11–13]. However, the possibility of forming Co–Cu alloys in the above structures did not practically produce an impact on the models used in describing the materials obtained. This should primarily be attributed to the extremely low concentration of cobalt in the Co–Cu alloys prepared in most of such experiments described by now, and, hence, to the extremely low magnetic ordering temperature of such a magnetic phase. It was shown [14] that homogeneous Co–Cu alloys are paramagnetic at Co concentrations below 25 at % and undergo transition to the spin-glass state below 20 K and that alloys with Co concentrations less than 10 at % are paramagnetic throughout the entire temperature range. Thus, close to room temperature, i.e., in the temperature interval of most applied interest for magnetic nanostructures, the effect of this phase on the magnetic and magnetic-transport properties of a sample can be safely neglected. A question can arise of whether this assumption is always valid? We demonstrate here that in some cases not only the naive model of a multilayer structure with perfect magnetic layers is incomplete to

account for the experimentally observed specific features of Co/Cu multilayers, but that the refinement of this model including in consideration the presence of a superparamagnetic phase [9] does not provide an insight deep enough to understand the phenomena occurring in such structures. Some technological conditions accepted in a sample preparation technique require taking into account the presence of a supersaturated Co–Cu alloy in the composition of the films studied.

Multilayer films with ultrathin magnetic layers have recently become a topic of great research interest because of their potential in designing high-sensitivity detectors of weak magnetic fields. Some studies revealed the possibility of increasing the low-field sensitivity of the GMR effect by using the so-called "quasi-granular multilayer films," in which the ferromagnetic layers consist of weakly coupled ferromagnetic grains, as is the case with granular materials [15, 16]. Besides, multilayers with ultrathin magnetic layers should reduce the probability of pinhole formation because of the small amount of the magnetic material they incorporate, which should likewise increase the low-field sensitivity and the maximum magnitude of the GMR effect. An improved low-field GMR sensitivity was reported to have been demonstrated in multilayer Cu(111)/$Ag_{67}Co_{33}$ samples, in which the $Ag_{67}Co_{33}$ layers represented a granular alloy. At a certain thickness of the copper layer, the magnetic particles at adjacent interfaces on opposite sides of the Cu layer featured antiparallel orientation, whereas the magnetic moments of particles inside the granular layer were oriented in a random way. The magnitude and field sensitivity of the effect increased with decreasing thickness of the AgCo layer because of the decreasing fraction of inner Co grains in the magnetic layer. A similar pattern was observed with the quasi-granular Fe/Ag multilayer layers [18]. A recent study reported of one more attempt of increasing the low-field sensitivity of the GMR effect in Co/Ag multilayers with fragmented magnetic layers [19].

The Co/Cu system revealed also that the magnetoresistance hysteresis decreases, and the sensitivity of the effect grows with decreasing thickness of the cobalt layer. High values of the GMR sensitivity combined with low hysteresis were observed [20] in multilayer structures with very thin cobalt layers (d_{Co1} = 3 Å) alternating with thicker (d_{Co2} = 15 Å) ones. Spizzo et al. [21] reported on the best magnetoresistance characteristics obtained with d_{Co} = 3–5 Å. With d_{Co} = 3 Å, the magnetic layers were fragmented, and the system revealed superparamagnetic properties. For d_{Co} = 4–5 Å, ferromagnetic order was already observed within the layers, despite the pattern of the latter still remaining fragmented. These multilayers were prepared at deposition rates of 0.4 and 0.6 Å/s for Co and Cu, respectively. At higher deposition rates, of the order of 8 Å/s, one prepared quasi-granular multilayer films which featured superparamagnetic behavior for d_{Co} = 4 Å [22]. Based on NMR data, Jerdyka et al. [23] reported on the decomposition of cobalt layers into clusters at d_{Co} = 6 Å.

We have to note, however, that formation of an alloy in the course of preparation of GMR structures based on the Co–Cu system, as well as the related aspect of controlling the quality of these structures, particularly of the thickness and structure of the interface, belong to problems still remaining largely unsolved. On the one hand, this stimulates an unending flow of studies aimed at an as complete as possible elucidation of the processes taking place during synthesis of the GMR structures; on the other, it provides a stimulus to further progress in development of a viable technology of preparation of granular films, multilayers, etc. There was, for instance, a report [24] about an efficient method of controlling the magnitude of the GMR effect in Co/Cu multilayer films by modifying the quality of the Co/Cu interface through successive annealing and bombardment of the film surface by high-energy ions.

We discuss here the properties of multilayer Co/Cu films with ultrathin Co layers prepared by DC magnetron sputtering, as well as the problem of a Co–Cu solid solution formation during sample preparation. We pay particular attention to the importance of taking this magnetic phase into consideration in dealing with the specific features in the magnetic and magnetic-transport properties of the material under study.

2. SAMPLE PREPARATION AND EXPERIMENTAL TECHNIQUE

Multilayer Co/Cu films were prepared by DC magnetron sputtering on glass substrates in an Ar atmosphere at room temperature. Two magnetron sources with cobalt and copper targets were fixed in the vacuum chamber such that they were isolated from the main volume of the chamber with the substrate holder, and from one another by metallic screens. Deposition of Co and Cu was effected through windows in the screen at the times when the substrates fixed to a rotating holder passed successively the corresponding magnetron sources. Thus, the material was deposited on the substrate only in the immediate vicinity of the sources. The amounts of the Co and Cu atoms deposited in one sputter cycle were defined by properly varying the opening of the corresponding window with a shutter. The base pressure in the chamber was 10^{-6} Torr, and the operating Ar pressure was 2×10^{-4} Torr. The deposition rate was ~3.5 Å/s for both sources. We prepared a series of samples with a nominal structure $[Co(d_{Co})/Cu(d_{Cu})]_n$, where the effective thickness of the Co layer was d_{Co} ~ 3.5 Å, and that of the Cu layer, d_{Cu}, was varied from 10 to 30 Å in steps of about 2 Å. The number of bilayers n of a multilayer structure was the same for all the samples, n = 100.

The structure of the samples thus prepared was studied with a DRON-4 X-ray diffractometer and a JEOL JEM-2010 transmission electron microscope. The chemical composition of the films was monitored by the X-ray fluorescence method, and that of the films studied by TEM, by energy dispersive spectral analysis as well. The magnetic characteristics were studied by means of an MPMS SQUID magnetometer (Quantum Design). The magnetoresistance characteristics were derived by the standard four-probe technique and by a method of magnetoresistance measurement in weak AC fields proposed by us earlier [25]. The temperature and field dependences of the resistance, $R(T)$ and $R(H)_{T=\text{const}}$, were probed with a PPMS instrument (Quantum Design) for studying physical properties.

The exact thicknesses of the Co and Cu layers were calculated from data on the chemical composition of the films obtained by the X-ray fluorescence method. It was found that the true thicknesses of the layers deviate slightly, by ~0.2–0.3 Å, from the values set by the sputtering conditions. Thus, the effective thickness of a Co layer ranged within 3.2–3.7 Å. As we shall see later on, for the samples under study here it is the value of d_{Co} (rather than that of d_{Cu}) that accounts primarily for their physical properties, so that even slight deviations of d_{Co} translate into noticeable variations in the fractions of the magnetic phases in a sample.

3. EXPERIMENTAL RESULTS

3.1. Structural Studies

X-ray diffraction measurements showed the samples under study to have fcc crystal structure. The lattice parameter calculated from the X-ray studies was found to fit that of bulk fcc copper. No indication of the presence of any texture was detected. One likewise did not detect any additional reflections, or shifts of those present, which could suggest the presence or effect of cobalt atoms on the crystal structure of any of the samples studied. This is in no way an unexpected finding, if one recalls the total amounts of cobalt and copper in a film. A more comprehensive investigation of the structure of the samples was conducted by TEM.

The electron microscope studies showed all the samples to have a similar structure. All films were nanocrystalline, with a broad grain size distribution, ranging from very small (~15–20 Å) to the largest (~150 Å) dimensions. The average grain size was ~80 Å. The electron diffraction patterns likewise were typical for such materials and featured a set of rings, whose positions of intensity maxima were in accord with the fcc structure, with the cell parameter equal to that of bulk copper. No effect of the presence of Co atoms on the crystal structure was also revealed. The width of the diffraction rings was, however, in excess of the difference between the lattice constants of cobalt, a_{Co}, and copper, a_{Cu}: $\eta = \dfrac{a_{Cu} - a_{Co}}{a_{Co}} = 2\%$. The large ring width can be readily interpreted in view of the size effect originating from the presence of a large number of crystallites with sizes of ~15–20 Å. Thus, while TEM measurements provide direct evidence for the presence of an fcc crystallographic phase only, with a lattice parameter equal to that of bulk copper, one should not exclude the possibility of existence of other phases as well, for instance, of grains of pure Co or of the Co–Cu alloy, which could be obscured by the diffraction rings of the main phase. In view of the method used to prepare the samples, one could venture a guess that cobalt deposited in layers with an effective thickness of less than two monolayers forms the smallest grains of those observed in the images obtained.

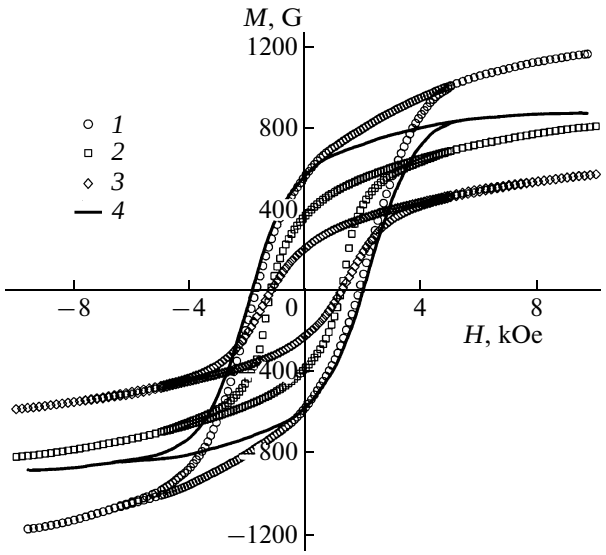

Fig. 1. Typical hysteresis loops of the Co/Cu films studied at $T = 5$ K. Composition of Co/Cu films, Å: (*1*) 3.7/18.7, (*2*) 3.3/10.7, (*3*) 3.2/16.3, and (*4*) loop for the $[3.7_{Co}/18.7_{Cu}]$ sample obtained after subtraction of the paramagnetic phase contribution from the original loop (see text).

3.2. Magnetic Measurements

Figure 1 shows typical low-temperature loops of the Co/Cu films (the magnetization M was calculated for the volume of Co in the sample). One clearly recognizes the ferromagnetic character of the dependences $M(H)$; however, it is clear that, in the field $H =$ 10 kOe, the magnetization does not reach saturation. The shape of the hysteresis loops reproduces well the Stoner–Wohlfarth plot for an ensemble of single-domain particles with randomly distributed easy magnetization axes. The absence of saturation can be caused by the presence of a paramagnetic phase in the composition of the samples under investigation, i.e., by single Co atoms or small cobalt clusters embedded

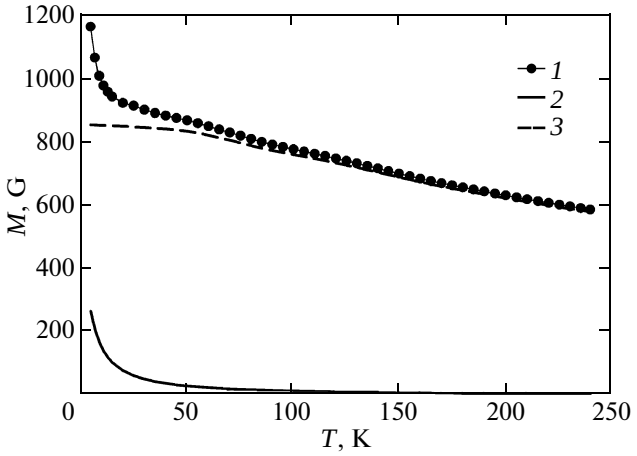

Fig. 2. (*1*) Experimental dependence $M(T)$ for the $[3.7_{Co}/18.7_{Cu}]$ sample measured in an external magnetic field $H = 10$ kOe and possible contributions to magnetization due to the (*2*) low-temperature paramagnetic phase and (*3*) all other magnetic phases.

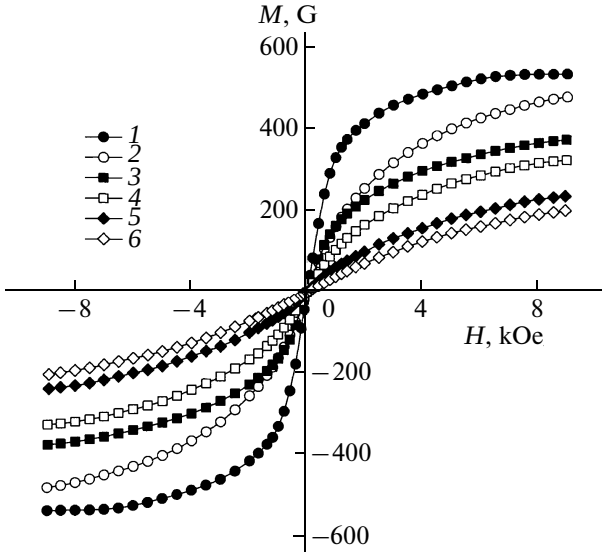

Fig. 3. Typical dependences $M(H)$ obtained for Co/Cu samples of different compositions at room temperature. The curves $M_{\|}(H)$ and $M_{\perp}(H)$ are referenced, respectively, as *p* and *n*. The Co/Cu film structure, Å: (*1*) 3.7/18.7, *p*; (*2*) 3.7/18.7, *n*; (*3*) 3.3/10.7, *p*; (*4*) 3.3/10.7, *n*; (*5*) 3.2/16.3, *p*; and (*6*) 3.2/16.3, *n*.

in the copper matrix, for which the dependence $M(H)$ is described by the Langevin law. Figure 2 plots the temperature dependence of the magnetization for the particular example of the $[3.7_{Co}/18.7_{Cu}]$ sample obtained in a field $H = 10$ kOe. This plot is typical of all the samples studied. One clearly sees that the magnetization rapidly decreases in the low-temperature region in the vicinity of the liquid-helium temperature, which can likewise serve as an indication of the presence of a paramagnetic phase in the sample.

Figure 3 shows the typical dependences $M(H)$ obtained at room temperature. All the samples are seen to reveal the superparamagnetic signature with no hysteresis and a noticeable magnetization in the field $H = 10$ kOe. The differences between the $M_{\|}(H)$ and $M_{\perp}(H)$ field dependences obtained in measurements in the film plane and along its normal, respectively, can be traced to the anisotropy in the shape of magnetic grains. A typical superparamagnet with spherical grains and randomly distributed easy magnetization axes is fully isotropic. In the case of the layer-by-layer deposition, the clearly pronounced shape anisotropy of the magnetic grains is in no way unexpected. The grains are oblate in the direction of the normal, and the related change in the demagnetizing factor gives rise to a difference between the curves $M_{\|}(H)$ and $M_{\perp}(H)$ (Fig. 3).

It is known that superparamagnetic behavior is characteristic of a system of noninteracting small ferromagnetic particles provided the internal energy of ferromagnetic interaction is much less than the thermal energy, $KV \ll k_B T$, where K is the anisotropy constant, and V is the particle volume. As a result, spontaneous magnetization of a sample is zero at any moment of time, as is remanence. When a sample is cooled below the critical point called the blocking temperature T_B, thermal energy becomes negligibly small, thus permitting the system to be described in terms of a model of single-domain noninteracting particles; within the hysteresis loop, remanence and coercivity $H_c \sim H_a/2$, where H_a is the anisotropy field, appear. The superparamagnetic blocking temperature T_B, which is a measure of the magnetic anisotropy energy, is quite often determined by comparing the temperature dependences of magnetization measured in a weak magnetic field following a preceding cooling of the sample in zero field (ZFC) and in the field in which the measurement is conducted (FC—field cooling).

Typical ZFC and FC dependences are shown in Fig. 4. Strange though it may seem, these two curves do not exhibit visible distinctions. Hence, the naive model assuming the samples studied to be superparamagnetic either breaks down altogether or is incomplete.

4. DISCUSSION OF THE RESULTS

4.1. Results of Magnetic Measurements

An analysis of the temperature and field dependences of the magnetization leads to the following conclusions.

(1) Assuming the presence of a paramagnetic phase, one can estimate the fraction of Co atoms it is comprised of, and correct the low-temperature $M(H)$ loops by subtracting the contribution due to this phase. The sharp drop of magnetization in the initial region

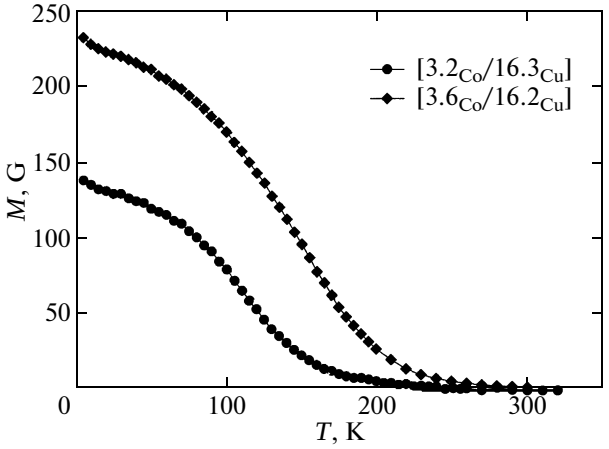

Fig. 4. Temperature dependences of the magnetization obtained in the FC and ZFC experiments conducted in an external field $H = 70$ Oe on two samples. Experimental points obtained in the two regimes coincide, to make the curves both FC and ZFC simultaneously.

of the $M(T)$ temperature dependences (Fig. 2) should obey the Langevin law

$$M = n\mu_m L(s), \qquad (1)$$

where μ_m is the magnetic moment of the paramagnetic particle, n is the concentration of magnetic moments, $s = \dfrac{\mu_m H}{k_B T}$, and $L(s)$ is the Langevin function

$$L(s) = \coth s - \frac{1}{s}.$$

By approximating the initial part of the experimental $M(T)$ curve by function (1), one can derive the contribution due to the paramagnetic phase to the total magnetization of a sample (see Fig. 2 for illustration). The average particle magnetic moment μ_m can be deduced from the fitting parameters; the value of μ_m estimated in this way was found to lie in the 9–15 μ_B interval for all samples, with the effective thickness of the cobalt layer d_{Co} producing the most essential effect on μ_m. In bulk cobalt, the magnetic moment is $\mu_{Co} = 1.85\ \mu_B$ per atom [26] ($\mu_{Co} = 1.68\ \mu_B$ for fcc Co with the lattice parameter equal to that of bulk copper); for small Co clusters embedded into the Cu matrix, however, the magnetic moment decreases down to 1 μ_B for a single atom [27, 28]. Thus, estimation of the average number of atoms making up clusters yields values ranging from $N_1 = 9/1.3 \approx 7$ to $N_2 = 15/1.5 \approx 10$ atoms, assuming $\mu_{Co} = 1.3$–$1.5\ \mu_B$ for clusters of this size. Knowing the contribution of the paramagnetic phase to the $M(T)$ curve, we can now estimate the fraction of Co atoms comprised in this phase. Estimation yields for all samples values lying within 30–45% of the total amount of cobalt. This approach, however, can be not accurate enough, because it assumes decomposition of $M(T)$ curves into two components only, the paramagnetic one, which is described by the Langevin law, and the ferromagnetic phase, which is saturated (or is close to saturation) in the low temperature region. In the case where the real structure of the samples differs from the model accepted here, the errors associated with the use of this decomposition should grow; nevertheless, based on the analysis of all results of the magnetic measurements (see below), we believe that application of this model should be valid in our case. The results obtained will hopefully permit us to arrive at a quantitative evaluation of the phase composition of the samples studied.

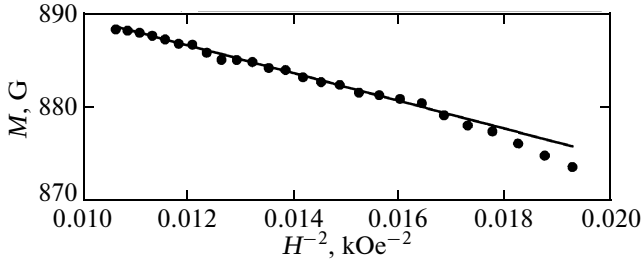

Fig. 5. Typical dependence of the magnetization $M(H^{-2})$ for the $[3.7_{Co}/18.7_{Cu}]$ sample. $T = 5$ K.

(2) On subtraction of the contribution due to the paramagnetic phase, the $M(H)$ curves measured at helium temperatures take on a typically ferromagnetic character (Fig. 1). It can be shown that the magnetization M for all samples approaches saturation following the functional dependence $M \sim H^{-2}$ (Fig. 5). This type of approaching saturation is characteristic of an ensemble of single-domain, weakly interacting magnetic particles. In this case, the high-field part of the curve can be described by the law of Akulov [29, 30]

$$\frac{|M(H) - M_s|}{M_s} = \left(\frac{D^{1/2} H_a}{H}\right)^2, \qquad (2)$$

where M_s is the saturation magnetization, H_a is the local anisotropy field, and D is a numerical symmetry coefficient which in the case of uniaxial anisotropy assumes the value $D = 1/15$. Approximating the experimental $M(H)$ curves with function (2), we obtained values of the local anisotropy field which lie within $H_a \sim 4$–5 kOe for all samples, and of the saturation magnetization varying from 440 to 900 G (here the magnetization was calculated for the total volume of cobalt in the sample). Reduction to the volume of Co making up the ferromagnetic phase (by subtracting the fraction corresponding to the paramagnetic phase) yielded the values for M_s within the interval of 800–1300 G. A comparison of the magnitude of M_s of the ferromagnetic phase for different samples revealed a clearly pronounced dependence of M_s on the effective thickness of the cobalt layer d_{Co}; indeed, the smallest

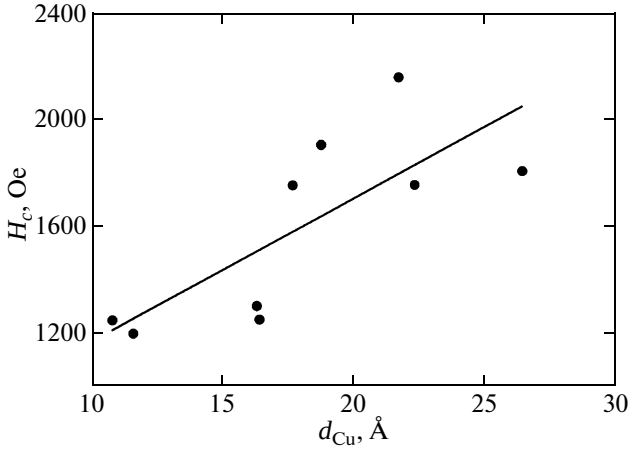

Fig. 6. Dependence of the coercive force of the ferromagnetic phase on the effective thickness of the copper layer d_{Cu}. $T = 5$ K. The solid line traces a linear dependence.

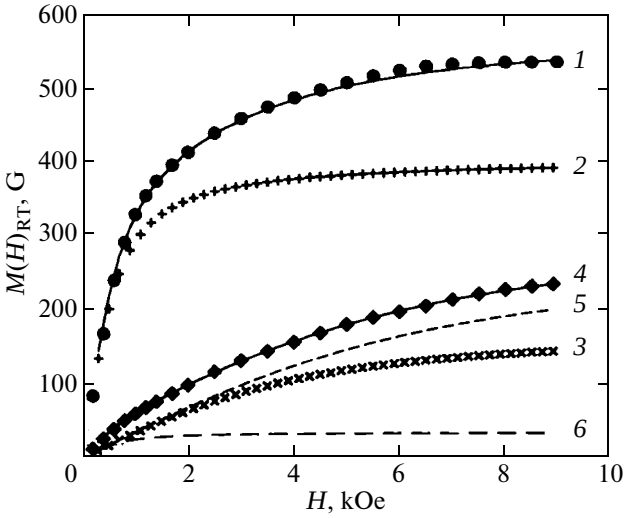

Fig. 7. Illustration of fitting of experimental curves $M(H)_{RT}$ by superposition of two Langevin functions corresponding to two main particle sizes. Curve *1*: circles are experimental points for the sample $[3.7_{Co}/18.7_{Cu}]$, and the solid line indicates the superposition of two Langevin functions shown separately by curves *2* and *3* for the large and small particles, respectively. Curve *4*: rhombi are experimental points for the sample $[3.2_{Co}/16.3_{Cu}]$, and the solid line represents the superposition of two Langevin functions shown separately by curves *5* and *6* for the small and large particles, respectively. See text for explanation.

value was obtained for the $[3.2_{Co}/16.3_{Cu}]$ sample with the thinnest Co layer thickness, and the largest value of M_s, for the $[3.7_{Co}/18.7_{Cu}]$ sample with the largest value of d_{Co} among the samples studied. The value of M_s for the other samples varied between these two values, depending on d_{Co}. The coercive force grew with increasing d_{Cu} from H_c = 1250 Oe for the $[3.3_{Co}/10.7_{Cu}]$ sample to H_c =2100 Oe for the $[3.5_{Co}/21.7_{Cu}]$ sample (Fig. 6). The scatter of experimental points on both sides of the straight line in Fig. 6 originates primarily from the variation in d_{Co} and H_a among different samples.

(3) Despite the clearly pronounced superparamagnetic character of the $M(H)$ curves measured at room temperature, they defy approximation with the Langevin function, which most probably should be assigned to the particles being distributed in size. In this case, fitting experimental $M(H)$ curves requires more than one Langevin function. As is evident from the shape of the $M(H)$ curves (Fig. 3), the distribution of magnetic particles in size is different for different samples. Determination of the exact character of this distribution is anything but a simple problem [31]. As this was shown earlier (see, e.g., [32]), however, in the case of a broad scatter in particle size, bimodal distribution is a model that quite frequently suits well in describing the behavior of a superparamagnetic system. Figure 7 illustrates the use of this model for two samples which differ most in their $M(H)$ dependences (Fig. 3).

Because each superparamagnetic particle consists of a large number of atoms, it can be suggested that the saturation magnetization of such a particle should coincide with that of bulk cobalt. Then for the $[3.7_{Co}/18.7_{Cu}]$ and $[3.2_{Co}/16.3_{Cu}]$ samples (Fig. 7) the characteristic particle dimensions derived from the model assuming bimodal distribution will be $D_1 \approx 32$ Å (~1.5×10^3 atoms) and $D_2 \approx 59$ Å (~9×10^3 atoms), which yields for the ratio of the numbers of atoms comprised in the corresponding phases $N_1/N_2 \approx 0.44$ for the first sample and $D_1 \approx 28$ Å (~900 atoms), and $D_2 \approx 58$ Å (~8.5×10^3 atoms), $N_1/N_2 \approx 8$ for the second sample. The above figures permit an estimate of the blocking temperature as 1/25 of the energy barrier associated with the magnetic anisotropy energy [32]

$$T_B = \frac{\Delta E}{25k_B} = \frac{K_U V}{25k_B}, \qquad (3)$$

where K_U is the anisotropy constant, and V is the particle volume. Recalling the value of the uniaxial anisotropy field $H_a \sim 5$ kOe derived from an analysis of the behavior of the $M(H)$ and K_U low-temperature curves approaching saturation, one comes to $K_U = \frac{H_a M_s}{2}$. We followed this approach to derive the blocking temperatures T_{B1} and T_{B2} relating, respectively, to the systems of "small" and "large" particles, which were found to be $T_{B1} \approx 17$ K and $T_{B2} \approx 100$ K for the $[3.7_{Co}/18.7_{Cu}]$ sample, and $T_{B1} \approx 10$ K and $T_{B2} \approx 95$ K for the $[3.2_{Co}/16.3_{Cu}]$ sample.

To obtain a physical pattern that would approximate as close as possible the real structure of the samples studied, one has to take into account the anisotropy of the shape of superparamagnetic particles, as

well as the possible variation in K_U with temperature. The analysis described in the present Section is aimed, however, primarily at estimating the parameters of the superparamagnetic phase and providing an insight into the problem of the phase composition of the samples under study. A more comprehensive analysis of the magnetization curves and exact calculation of the parameters of the magnetic phases is beyond the scope of the present paper and is deferred until a later publication.

(4) The behavior of the dependences $M(T)$ measured in the magnetic field $H = 70$ Oe (Fig. 4) can be understood by accepting the possibility of formation of the Co–Cu alloy phase. Indeed, the Curie temperature of the Co_xCu_{100-x} alloy is below the room temperature for $24 \le x \le 34$ [14]. The low-temperature $M(H)$ curves described in [14] corresponded to a high magnetic susceptibility of the alloy in weak fields; indeed, at $H = 70$ Oe the magnetization was at least $M_s/2$. Obviously enough, the $M(T)$ curves measured in a field $H = 70$ Oe reflect the temperature dependence of the magnetization of this phase. Thus, even above the blocking temperature of the largest superparamagnetic particles but below the ordering temperature T_c of the Co–Cu alloy phase, the system, rather than being a "pure" superparamagnet, is at least a "mixture" of superparamagnetic and ferromagnetic regions. An increase in the temperature above T_c brings about disruption of exchange coupling for the Co–Cu phase, with the system transferring to the superparamagnetic phase if $T_B < T_c$. The Curie temperature of the alloy can be extracted from the characteristic slope of the dependences $M^2(T)$. The Curie temperatures estimated in this way range from ~120 to ~250 K for different samples. In all the cases studied, the inequality $T_B < T_c$ was indeed satisfied. One established a correlation between T_c and the effective thicknesses of the magnetic and nonmagnetic layers; indeed, it was found that both an increase in d_{Co} and a decrease in d_{Cu} lead to an increase in T_c, and vice versa. The typical "tail" in the $M(T)_{H=70\,\text{Oe}}$ curves above T_c derives from the response of superparamagnetic particles, exactly as expected from the Langevin law. The very high local anisotropy fields of ~4–5 kOe for fcc cobalt derived from an analysis of the relation describing the approach to saturation are most probably associated with the smallness of the magnetic particles, because such factors as surface anisotropy and lattice strains can give rise to a substantial growth of magnetic anisotropy in the case of small grains.

4.2. Magnetoresistance

The dependences $R(H)$ measured at temperatures above T_c of the Co–Cu alloy phase are typical of a granular alloy with superparamagnetic behavior, namely, in the field $H = 50$ kOe (the maximum field achievable in the experiment) saturation was not reached. Lowering the temperature below the point of ordering of the above magnetic phase brought about the appearance of hysteresis in the $R(H)$ curves, which became increasingly pronounced with further lowering of the temperature, reaching the maximum value at the lowest temperature $T = 2$ K used in these experiments. At $T = 5$ K, the curves $R(H)$ correlated well with the dependences $M(H)$ of the corresponding samples; indeed, the falling and rising branches of the curves crossed in fields equal to the coercive force derived from the $M(H)_{T=5\,\text{K}}$ curves. At $T = 2$ K, magnetoresistance still did not reach saturation in a field $H = 50$ kOe. The typical values of the magnetoresistance effect were found to be $MR_{H=50\,\text{kOe}} \sim 10$–$20\%$ at 5 K and 5–10% at 250 K.

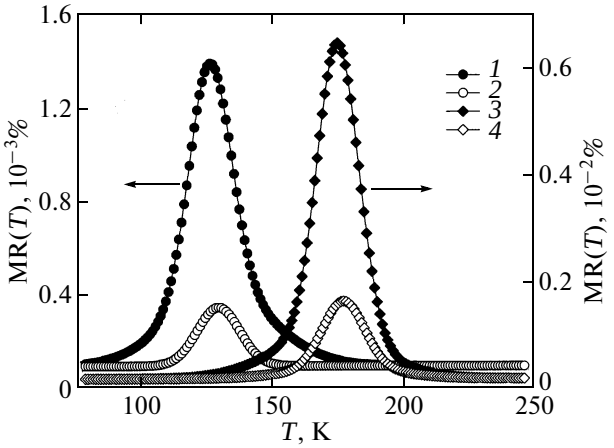

Fig. 8. Temperature dependences of the magnetoresistance MR(T) of the (*1*, *2*) $[3.2_{Co}/16.3_{Cu}]$ and (*3*, *4*) $[3.6_{Co}/16.2_{Cu}]$ samples measured in weak AC fields. H, Oe: (*1*, *3*) and (*2*, *4*) 2.

The most interesting results were obtained in measurements of the low-field dependences MR(T) in an AC magnetic field; indeed, we succeeded in detecting a clearly pronounced maximum in magnetoresistance at temperatures practically coinciding with those of ordering of the Co–Cu alloy phase, which were derived from an analysis of the dependences $M(T)_{H=70\,\text{Oe}}$. Figure 8 shows the curves MR(T) of the samples for which the dependences $M(T)_{H=70\,\text{Oe}}$ are presented in Fig. 4. The difference between the temperature of the maximum in magnetoresistance, T_{max}, and T_c estimated from $M(T)_{H=70\,\text{Oe}}$ curves did not exceed 7 K for all the samples. We believe this result to provide persuasive support for our earlier assumption of the presence in the composition of the samples under study of the Co–Cu alloy phase; in this case, the maximum of magnetoresistance can be identified with the temperature of the magnetic phase transition of the phase of this alloy and attributed to deviation of the magnetic susceptibility at this point. The slight difference between the values of T_c obtained from an

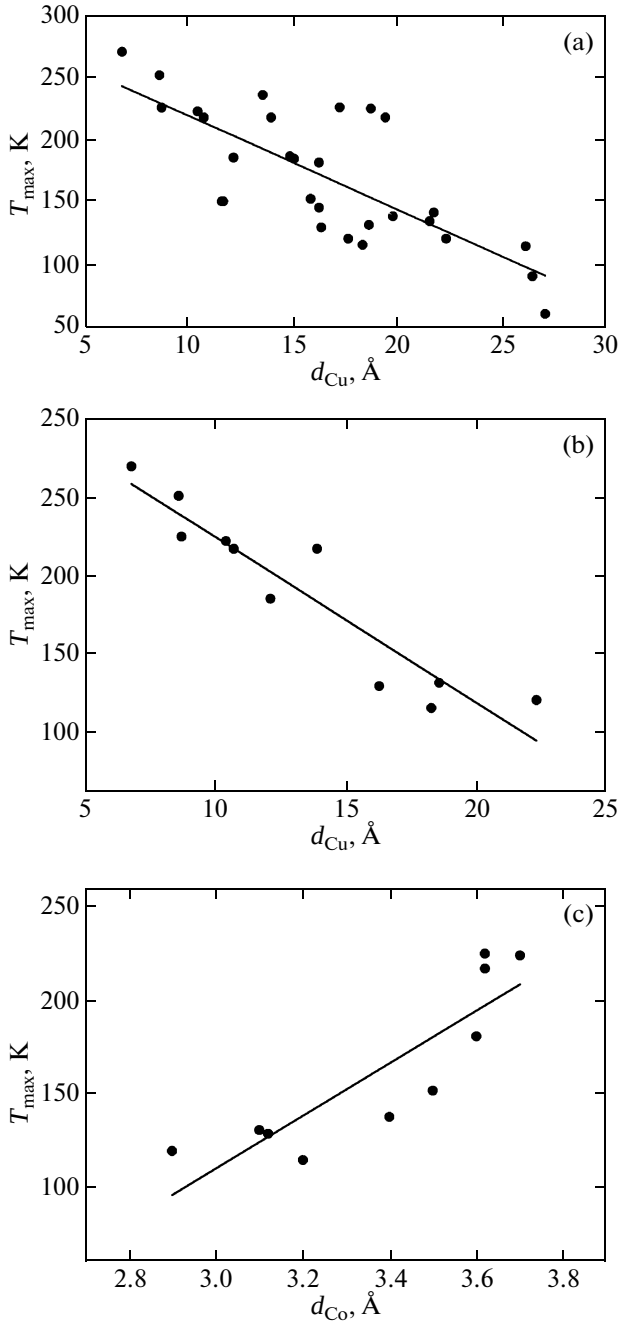

Fig. 9. Dependences of the temperature of the maximum of the magnetoresistance in a weak AC magnetic field on the quantities d_{Cu} and d_{Co}: (a) the total dependence of T_{max} on d_{Cu} for all the samples studied, (b) the same dependence but only for samples with close values of the effective thickness of the Co layer (d_{Co} = 3.2–3.3 Å), and (c) the dependence of T_{max} on d_{Co} for samples with d_{Cu} = 16–19 Å. Solid lines indicate the linear approximation of the experimental points.

analysis of the $M(T)_{H=70\,Oe}$ and MR(T) curves can be assigned to the fairly approximate method of T_c determination employed in the first case, in view of the fact that the magnetization of the Co–Cu alloy probably did not reach saturation in the field of 70 Oe, as well as of the possible effect of other magnetic phases on the pattern of the $M(T)_{H=70\,Oe}$ curves. For all samples, the values of T_{max} ranged from 130 to 250 K, and were found to depend on both parameters, d_{Co} and d_{Cu} (Fig. 9). An increase in d_{Co}, as a decrease in d_{Cu}, brought about increase in this temperature, and conversely, a decrease in d_{Co} and an increase in d_{Cu} reduced T_{max}. The ordering temperature range of the Co–Cu alloy, 130–250 K, offers a possibility of estimating the Co concentration in the alloy as ~30 at %. According to the magnetic phase diagram presented in [14], the ordering temperature $T_c \approx 130$ K corresponds to a Co concentration $x \approx 28$ at %, and $T_c \approx 250$ K, to $x \approx 32$ at %. The temperature dependences of the electrical resistance R exhibited a clearly metallic signature by growing linearly with temperature; however, the $R(T)$ curves had a feature suggesting a change in the temperature coefficient of resistivity at T_{max}. This coefficient decreased by 5–20% for different samples. Such a feature can also be expected to appear if a magnetic phase transition takes place at this temperature.

The measured values of T_{max} and, accordingly, the ordering temperatures of the Co–Cu alloy turned out to be very stable and did not vary with time, thus suggesting a constancy of its composition and physical properties. The MR(T) curves measured one year after the sample preparation coincided completely with the corresponding curves obtained on as-prepared samples (the samples were stored during this time in normal conditions, in atmosphere, at a temperature $t \sim$ 20°C and humidity of ~50%). By contrast, experiments involving heating brought about totally different results; indeed, annealing at a temperature $t = 100$°C for 15 min resulted in a noticeable decrease in the magnetoresistance effect in magnitude at T_{max}, while annealing at $t = 100$°C for 1.5 h culminated in a complete disappearance of the MR peak. Obviously enough, even at a temperature $T = 100$°C, the alloy undergoes decomposition, which leads to the total segregation of cobalt and copper.

4.3. Decrease in the Cobalt Layer Thickness d_{Co}

In an attempt to clarify the effect of magnetic layer thickness on the structure of the samples and their physical properties, we prepared a [$2.9_{Co}/17.6_{Cu}$] sample with the d_{Co} thickness smaller than those in the samples studied earlier. On this sample, we measured the same magnetic characteristics as on the others, and they confirmed that this sample had similar characteristics. While we detected all the three abovementioned magnetic phases, their parameters and the relative numbers of Co atoms they were formed of were different. The major fraction of magnetic atoms was found to be contained in the smallest magnetic grains whose blocking temperature T_B was close to liquid-

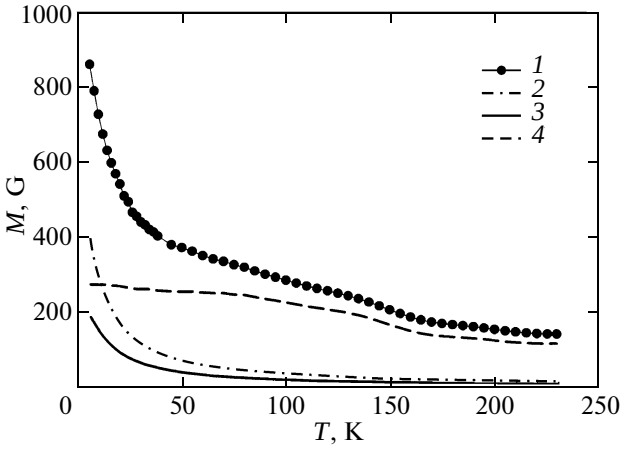

Fig. 10. (*1*) Experimental dependence $M(T)$ for the $[2.9_{Co}/17.6_{Cu}]$ sample measured in an external magnetic field $H = 10$ kOe and possible contributions to the magnetization due to (*2*, *3*) the magnetic phase originating from the presence of tiny magnetic particles in accordance with the bimodal distribution model and (*4*) all other magnetic phases.

helium temperature. Therefore, the $M(T)_{H=10\,\text{kOe}}$ curve for this sample could not be unfolded into two components, as this was done earlier for all samples with the cobalt layer thickness $d_{Co} \sim 3.5$ Å (Fig. 10). The size distribution of the smallest grains for this sample is certainly much broader, which makes the naive model based on an average (effective) grain size invalid. We invoked therefore the bimodal distribution model. Figure 10 illustrates the bimodal approximation for the $[2.9_{Co}/17.6_{Cu}]$ sample. The magnetic moment of the particles estimated from this deconvolution was found to be $\mu_{m1} \approx 29\ \mu_B$ and $\mu_{m2} \approx 38\ \mu_B$, and the number of Co atoms per such a particle was, respectively, $N_1 \approx 18$ and $N_2 \approx 24$. In view of the fairly extended temperature interval (up to ~50 K) in which one observed the sharp decrease in the magnetization, this estimate appears too rough, because a sample can contain a large number of grains with T_B in the 5–50-K interval, which affect the character of the low-temperature part of the dependence $M(T)_{H=10\,\text{kOe}}$ and make isolation of the contribution due to the "pure" paramagnetic phase a formidable problem. For the same reason, we have not succeeded in subtracting the contribution of the paramagnetic phase from the dependence $M(H)$ measured at liquid-helium temperature, which could have permitted us to derive the hysteresis loop due to the ferromagnetic phase, as this was done for the samples with $d_{Co} \approx 3.5$ Å. The $[2.9_{Co}/17.6_{Cu}]$ sample is also characterized by dependences $M(H)$ of the superparamagnetic type at room temperature, but the grain size deduced from the bimodal distribution model was found to be $D_1 \approx 28$ Å and $D_2 \approx 49$ Å (to be compared with the corresponding sizes for the $[3.2_{Co}/16.3_{Cu}]$ sample, $D_1 \approx 28$ Å and $D_2 \approx 58$ Å), the magnetization in the field $H = 10$ kOe was $M = 105$ G, and the MR(T) curve passed through a maximum at $T_{max} = 120$ K.

5. CONCLUSIONS

Drawing primarily from the results amassed in magnetic and magnetoresistance measurements, we have shown that multilayer Co/Cu films with ultrathin magnetic layers obtained by magnetron sputtering have a complex multiphase structure. The main phases are the paramagnetic phase associated with tiny (a few atoms altogether) Co clusters, the superparamagnetic phase originating from large (tens of angstroms) cobalt clusters, and the low-temperature ferromagnetic phase of a Co–Cu alloy with a Co concentration of ~28–32 at %. The main parameters of these phases, such as the size distribution of particles in the paramagnetic and superparamagnetic phases and the Co concentration in the Co–Cu alloy phase, just as the relative concentrations of Co atoms accounting for these phases, are mediated by the amount of the material deposited in one sputtering cycle, which, in its turn, is connected with the effective thicknesses of the layers, d_{Co} and d_{Cu}.

A decrease in d_{Cu}, and, to a larger extent, an increase in d_{Co} give rise to the following changes in the structure and physical properties of the samples studied. First, it brings about an increase in the number of Co atoms making up the larger magnetic grains and the associated increase in the saturation magnetization at $T = 5$ K. Second, this gives rise to a decrease in the relative number of Co atoms bound in the smaller grains, and a weakening of the paramagnetic effect at $T = 5$ K. And, finally, third, the Co concentration in the Co–Cu alloy grows and, accordingly, the Curie temperature of the given phase increases. An increase in d_{Cu} and a decrease in d_{Co} produce the opposite effect.

An interesting finding is observation of a strongly pronounced maximum in the low-field temperature dependences of magnetoresistance at the temperature of the magnetic phase transition in the Co–Cu alloy. Formation of an alloy with a fairly high Co concentration, which corresponds to the nonequilibrium region of the phase diagram, is in itself a remarkable effect; it can be traced to the specific features of the method employed in our study for sample preparation.

We have demonstrated that in order to gain a clear understanding of the physical properties of multilayer Co/Cu films with ultrathin magnetic layers produced by magnetron sputtering one should take into account the presence of the phase of metastable Co–Cu alloy in these films.

REFERENCES

1. S. S. P. Parkin, R. Bharda, and K. P. Roche, Phys. Rev. Lett. **66**, 2152 (1991).
2. A. E. Berkowitz, J. R. Mitchell, M. J. Carey, A. P. Young, S. Zhang, F. E. Spada, F. T. Parker, A. Hutten, and G. Thomas, Phys. Rev. Lett. **68**, 3745 (1992).
3. J. Q. Xiao, J. S. Jiang, and C. L. Chien, Phys. Rev. Lett. **68**, 3749 (1992).
4. T. Nishizawa and K. Ishida, Bull. Alloy Phase Diagrams **5**, 161 (1984).
5. E. Y. Tsymbal and D. G. Perrifor, Solid State Phys. **56**, 113 (2001).
6. U. Bovensiepen, P. Poulopoulos, W. Platow, M. Farle, and K. Baberschke, J. Magn. Magn. Mater. **192**, L386 (1999).
7. J. de la Figuera, J. E. Prieto, G. Kostka, S. Müller, C. Ocal, R. Miranda, and K. Heinz, Surf. Sci. **349**, L139 (1996).
8. M. Ø. Pedersen, I. A. Bönicke, E. Laegsgaard, I. Stensgaard, A. Ruban, J. K. Nørskov, and F. Besenbacher, Surf. Sci. **387**, 86 (1997).
9. I. Bakonyi, L. Péter, Z. Rolik, K. Kiss-Szabó, Z. Kupay, J. Tóth, L. F. Kiss, and J. Pádár, Phys. Rev. B: Condens. Matter **74**, 054427 (2004).
10. J. F. Bobo, H. Kikuchi, O. Redon, E. Snoeck, M. Piecuch, and R. L. White, Phys. Rev. B: Condens. Matter **60**, 4131 (1999).
11. J. C. S. Kools, W. Kula, D. Mauri, and T. Lin, J. Appl. Phys. **85**, 4466 (1999).
12. J. F. Bobo, L. Gabillet, and M. Bibes, J. Phys.: Condens. Matter **16**, 471 (2004).
13. H. D. Chopra, D. X. Yang, P. J. Chen, D. C. Parks, and W. F. Egelhoff, Jr., Phys. Rev. B: Condens. Matter **61**, 9642 (2000).
14. J. R. Childress and C. L. Chien, Phys. Rev. B: Condens. Matter **43**, 8089 (1991).
15. T. L. Hylton, K. R. Coffey, M. A. Parker, and J. K. Howard, Science (Washington) **261**, 1021 (1993).
16. M. Angelakeris, P. Poulopoulos, O. Valassiades, N. K. Flevaris, D. Niarchos, and A. Nassiopoulou, Sens. Actuators, A **91**, 180 (2001).
17. Y. Luo, M. Moske, A. Kaeufler, T. Lorenz, and K. Samwer, J. Appl. Phys. **81**, 4589 (1997).
18. J. Balogh, M. Csontos, D. Kaptás, and G. Mihály, Solid State Commun. **126**, 427 (2003).
19. V. K. Sankaranarayann, Om Prakash, and S. T. Lakshmikumar, J. Surf. Sci. Technol. **22**, 15 (2006).
20. D. J. Kubinski and H. Holloway, J. Magn. Magn. Mater. **165**, 104 (1997).
21. F. Spizzo, E. Angeli, D. Bisero, P. Vavassori, and F. Ronconi, Appl. Phys. Lett. **79** 3293 (2001).
22. R. Loloee, P. A. Schroeder, W. P. Pratt, Jr., J. Bass, and A. Fert, Physica B (Amsterdam) **204**, 274 (1995).
23. E. Jerdyka, M. Wojcik, S. Nadolski, D. J. Kubinski, and H. Holloway, J. Magn. Magn. Mater. **177–181**, 1183 (1998).
24. M. Cai, T. Veres, F. Schiettekatte, S. Roorda, and R. W. Cochrane, J. Appl. Phys. **95**, 2006 (2004).
25. P. D. Kim, D. L. Khalyapin, and L. E. Bykova, Prib. Tekh. Éksp., No. 4, 126 (2007) [Instrum. Exp. Tech. **50** (4), 547 (2007)].
26. S. V. Vonsovskii, *Magnetism* (Nauka, Moscow, 1971; Wiley, New York, 1974).
27. A. B. Klautau and S. Frota-Pessôa, Surf. Sci. **497**, 385 (2002).
28. R. N. Nogueira and H. M. Petrilli, Phys. Rev. B: Condens. Matter **63**, 12 405 (2001).
29. R. S. Iskhakov, S. V. Komogortsev, A. D. Balaev, and L. A. Chekanova, Pis'ma Zh. Tekh. Fiz. **28** (17), 37 (2002) [Tech. Phys. Lett. **28** (9), 725 (2002)].
30. H. Errahmani, N. Hassanaïn, A. Barrada, M. Abid, H. Lassri, G. Schmerber, and A. Dinia, J. Magn. Magn. Mater. **241**, 335 (2002).
31. A. Kákay, M. W. Gutowski, L. Takacs, V. Franco, and L. K. Varga, J. Phys. A: Math. Gen. **37**, 6027 (2004).
32. V. Franco and A. Conde, J. Magn. Magn. Mater. **277**, 181 (2004).

Translated by G. Skrebtsov